

Rectification in Supramolecular Zinc Porphyrin/Fulleropyrrolidine Dyads Self-Organized on Gold(111)

Francesca Matino,^[a] Valentina Arima,^{*[a]} Manuel Piacenza,^[a] Fabio Della Sala,^[a] Giuseppe Maruccio,^[a] Ray J. Phaneuf,^[a, b] Roberta Del Sole,^[c] Giuseppe Mele,^[c] Giuseppe Vasapollo,^[c] Giuseppe Gigli,^[a] Roberto Cingolani,^[a] and Ross Rinaldi^[a]

Self-assembled donor/acceptor dyads are of current interest as they are biomimetic to the natural photosynthetic conversion system. Herein, we present an ultrahigh-vacuum scanning tunneling microscopy and scanning tunneling spectroscopy (UHV-STM/STS) study of ex situ self-assembled supramolecular dyads consisting of fulleropyrrolidines (PyC₂C₆₀) axially ligated to zinc(II) tetraphenylporphyrin (ZnTPP), self organized on a 4-aminothiophenol (4-ATP) self-assembled monolayer on gold-(111). These dyads show both bias-polarity-dependent apparent height in STM images and highly rectifying behavior in

tunneling spectroscopy. First-principles density functional theory calculations clarify the conformational and electronic properties of the 4-ATP/ZnTPP/PyC₂C₆₀ system. Interestingly, we find easier tunneling for electrons moving from the acceptor side of the dyads to the donor side, in the inverse-rectifying sense with respect to previously reported molecular rectifiers. Such behavior cannot be explained as an elastic resonant tunneling process, but it can be by using a model based on the Aviram–Ratner mechanism.

1. Introduction

The major goal of molecular electronics^[1–4] is to use single molecules as active components in devices working as sensors, memories, and switches at a molecular level as an alternative to semiconductor-based nanoscale electronics. In this respect, photoactive devices have been extensively pursued,^[5] and in recent years donor/acceptor (D/A) dyads that undergo light-induced electron or energy transfer have been intensively investigated in order to exploit the possibility of mimicking the primary events of the photosynthetic reaction center and develop new functional nanodevices.^[6] Among the different routes to form dyads, self-assembly is particularly interesting, since it allows the organization of D/A building blocks at the molecular scale with a specific orientation on the surface.

In this respect, fullerenes are especially attractive as electron acceptors because of their three-dimensional structure, low reduction potentials, and absorption spectra which extend over most of the visible region.^[7–10] On the other hand, porphyrins and their derivatives, which act as electron donors, have excellent features as electron-transfer systems and the photosynthetic capability to convert light to energy.

The expected applications of porphyrin/fullerene dyads in molecular electronics have driven research in the field. Metal-to-ligand axial coordination between metal porphyrins and fullerenes functionalized with a pyridine group allows the creation of supramolecular D/A dyads with controlled geometry and long-lived charge-separated states.^[11–17] Recently, a self-assembly method involving zinc tetraphenylporphyrin (ZnTPP) and a C₆₀ derivative (a fulleropyrrolidine) using axial ligation of the central metal ion was described by D'Souza et al.^[6, 15, 18] The dynamics of the electron-transfer process in solution in both polar and nonpolar solvents is well known: steady-state and

time-resolved emission as well as transient absorption techniques have previously been employed to clarify the excited-state electron-transfer reactions.^[15, 18–23] Further recent investigations on self-assembled monolayers of covalently linked fullerene/porphyrin dyads on gold^[24] and indium tin oxide (ITO) surfaces have demonstrated photoinduced electron transfer, independent of the dyad orientation.^[25] Most interesting is the recent work of Nishino et al.^[26] in which they observe rectifying behavior for electron tunneling between a fullerene-terminated STM tip and single porphyrin molecules adsorbed on Au. In particular, they found electron tunneling from the porphyrin

[a] Dr. F. Matino,^{*} Dr. V. Arima, Dr. M. Piacenza, Dr. F. Della Sala, Dr. G. Maruccio, Prof. R. J. Phaneuf, Prof. G. Gigli, Prof. R. Cingolani, Prof. R. Rinaldi
National Nanotechnology Laboratory (CNR-INFM)
Distretto Tecnologico ISUFI, Università del Salento
via Arnesano, 73100 Lecce (Italy)
Fax: (+39) 832-298230
E-mail: valentina.arima@unile.it

[b] Prof. R. J. Phaneuf
Department of Materials Science and Engineering
University of Maryland and Laboratory for Physical Science
College Park, 20740 Maryland (USA)

[c] Dr. R. Del Sole, Dr. G. Mele, Prof. G. Vasapollo
Dipartimento di Ingegneria dell'Innovazione
Università del Salento
via Arnesano, 73100 Lecce (Italy)

[*] Current address:
Institut für Experimentelle und Angewandte Physik
der Christian-Albrechts-Universität Kiel
24118 Kiel (Germany)

Supporting information for this article is available on the WWW under <http://dx.doi.org/10.1002/cphc.200900371>.

on the surface to the fullerene derivative on the tip through intermolecular interaction, but not in the opposite direction: this indicates that the porphyrin/fullerene pair can act as a molecular rectifier.

Many different studies^[27–46] have been carried out to investigate rectification in transport through donor/acceptor unimolecular pairs and supramolecular assemblies, starting from the pioneering work of Aviram and Ratner.^[45] However, while some studies^[27,31,35–37,40,42] show a preferred direction for electron transport from acceptor to donor sites, in many investigations^[28,30,32–34,38,39,41,43] the electron flow is enhanced in the opposite direction (i.e., from donor to acceptor), as suggested by the work of Ellenbogen and Love.^[29] Here we address this fundamental issue both experimentally and theoretically in the case of isolated supramolecular dyads composed of a fulleropyrrolidine functionalized by a pyridyl group (PyC₂C₆₀) coupled to zinc(II) tetraphenylporphyrin (ZnTPP) molecules lying on a 4-aminothiophenol (4-ATP) monolayer self-assembled on an Au(111) surface (Figure 1). Scanning tunneling microscopy

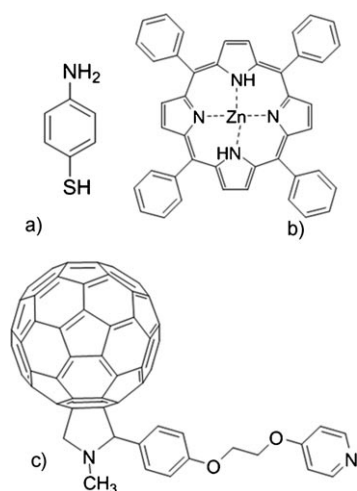


Figure 1. Molecular structures of a) 4-ATP, b) ZnTPP, and c) PyC₂C₆₀.

(STM) and spectroscopy (STS) were used to investigate the self-organized dyads, which showed both a bias-polarity dependence of the STM profiles and asymmetric, diodelike current/voltage characteristics with a rectification sense opposite to that observed by Nishino et al.^[26] By performing first-principles density functional theory (DFT) calculations for the 4-ATP/ZnTPP and 4-ATP/ZnTPP/PyC₂C₆₀ systems, we found that the lowest unoccupied molecular orbital (LUMO) is localized on the fullerene, while the highest-occupied molecular orbital (HOMO) is localized on the porphyrin ring. The observed rectifying behavior is thus explained within the Aviram–Ratner mechanism.

2. Results and Discussion

2.1. Experimental Results

Scanning tunneling microscopy images of the 4-ATP/ZnTPP/PyC₂C₆₀ system were acquired in constant-current mode with

tunneling currents of 50 pA and sample bias in the range from ± 1 to ± 2 V (Figure 2). Bright spots/protrusions are clearly visible on the surface (Figure 2a), with lateral dimensions of $2.0 \pm$

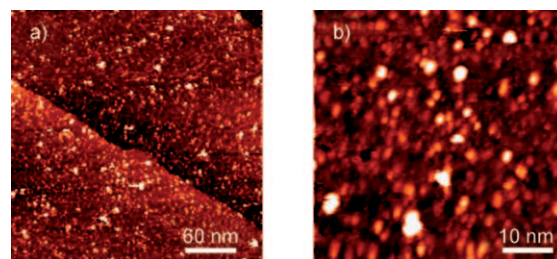


Figure 2. STM images from a dilute ZnTPP/PyC₂C₆₀ sample, acquired with a Pt/Ir tip at a) $V_{\text{set point}} = +2$ V, $I_{\text{set point}} = 50$ pA, scan area: 300×300 nm, and b) $V_{\text{set point}} = +1.6$ V, $I_{\text{set point}} = 50$ pA, scan area: 50×50 nm.

0.5 nm in diameter and 0.4 ± 0.1 nm in apparent height (Figure 2b). We attribute these protrusions to the fullerene moiety of ZnTPP/PyC₂C₆₀ dyads, due to the observed lateral sizes and their narrow distribution, which would be unlikely for clusters. Taking into account tip-convolution effects, the lateral dimensions of the protrusions are within the range reported for C₆₀ on various substrates.^[47,48] On the other hand, the apparent height is smaller than the nominal 1.1 nm estimated for the fullerene from molecular van der Waals dimensions,^[49] but this value in STM measurements is well known to depend on the density of states near the Fermi level.^[50] The height is also slightly smaller than that of about 0.5–0.6 nm reported from STM measurements on C₆₀ on metal surfaces.^[48,51] However, as we demonstrate below, the apparent height of dyads was found to strongly depend on the tunneling conditions, although an influence of the spatial orientation also exists (see the extreme calculated conformations shown in Figure 5 below). In particular, we observed a significant dependence on the bias polarity, as shown in the line profiles of Figure 3. Dyads appear less high when negative bias voltages are applied to the sample: the apparent heights measured at -1.6 V

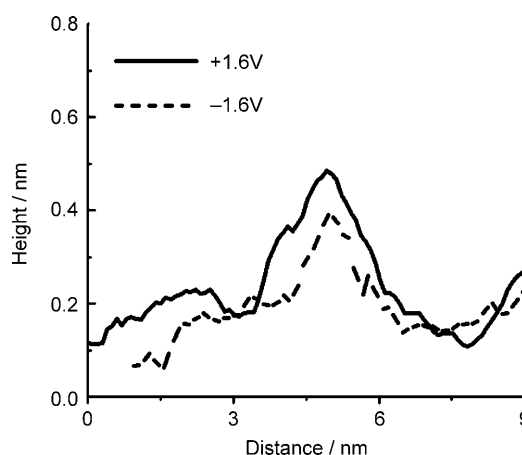


Figure 3. Cross-sectional height profiles acquired across a ZnTPP/PyC₂C₆₀ dyad.

are approximately 20% less than those at +1.6 V. In contrast, the apparent heights of the smaller structures visible on the surface, presumably porphyrin molecules uncomplexed with fullerenes, are rather independent of the bias polarity.

Figure 4 compares current/voltage (I/V) curves measured above dyads with those of uncomplexed porphyrins. In the case of dyads, the characteristics are asymmetric, with higher

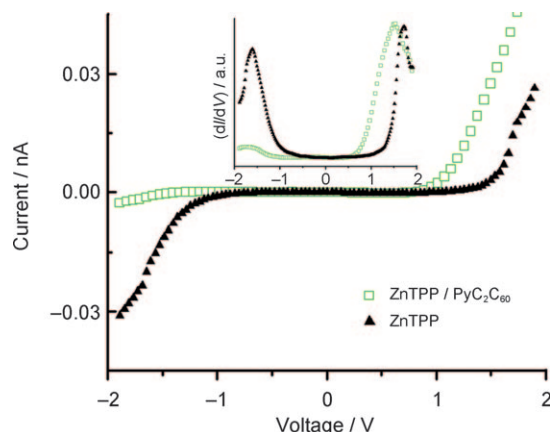


Figure 4. Typical I/V curves collected through a ZnTPP/PyC₆₀ dyad (green) and from a nearby ZnTPP structure (black). The sample set-point voltage is +2 V, and the current demand 50 pA. Inset: derivatives dI/dV of the same curves.

current at positive sample voltages, while I/V curves measured above the porphyrins are nearly symmetric. We find this result to be both unambiguous and reproducible. Using the ratio $R(V) = 2[|I(+V)| - |I(-V)|] / (|I(+V)| + |I(-V)|)$ to quantify the asymmetry in I/V curves, we find $R = 1.83$ for $V = 1.8$. Using the standard definition of $RR = |-I(V)/I(-V)|$ we obtain a value of about 24, but this value is strongly dependent on voltage. Figure S1 of the Supporting Information shows a histogram of the rectification ratio in our samples calculated by using the first definition. In agreement with the report of Nishino et al. for moieties in tunneling contact, the rectification observed here for supramolecular assemblies seemingly arises from asymmetry in transport through the donor/acceptor molecule dyads. However, whereas Nishino et al. reported higher currents at negative substrate voltage, we observed higher tunneling currents at positive substrate voltage. The inset of Figure 4 shows the differential conductance calculated from the two I/V curves shown. Extrapolating the tangent of the steeply rising edges of the conductance well downward to zero yields onsets at approximately +0.7 and -1.2 eV for transport through the dyad; similar extrapolations for the 4-ATP/ZnTPP complex yields thresholds at approximately +1.2 and -1.0 eV. Based on this, we estimate the energy gap for the 4-ATP/ZnTPP/PyC₆₀ structure to be approximately 1.9 eV, while for the 4-ATP/ZnTPP layer we estimate approximately 2.2 eV. These values are in agreement with electrochemical measurements on similar systems.^[18]

2.2. Theoretical Results

2.2.1. Molecular Geometries

Figure 5 shows the DFT-optimized molecular geometry of the 4-ATP/ZnTPP/PyC₆₀ structure. The structure is attached to a gold (111) substrate as described in ref. [52], that is, with an angle of 20° between the 4-ATP plane and the gold substrate.

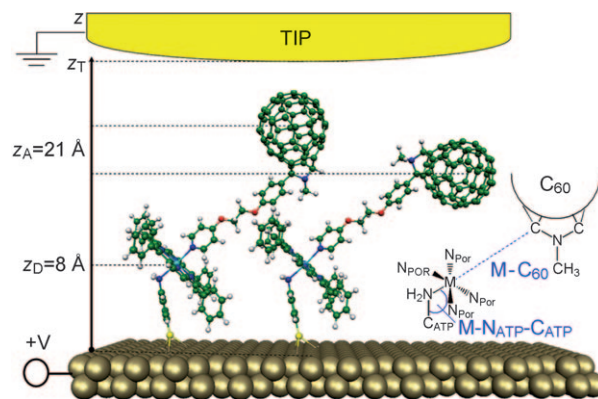


Figure 5. DFT energy-optimized molecular geometry for 4-ATP/ZnTPP/PyC₆₀ (two different isomers) on gold substrate, molecular distance with respect to the substrate, STM configuration, and the most important geometrical parameters listed in Table 1.

The fullerene subsystem is free to rotate around the C₂ axis. In Figure 5, the two extreme orientations with different fullerene–substrate distances z_A are shown. The energetic difference of the two rotamers at the B3-LYP/SV(P) level is negligible (0.46 kcal mol⁻¹). The average distance between the center of the fullerene and the metal substrate is $z_A = 21$ Å. Figure 5 also shows the STM configuration schematically.

Table 1 reports the main geometrical parameters, defined on the right-hand side of Figure 5. The plane of the metalloporphyrin is tilted relative to the 4-ATP plane, as it was shown in a previous study on 4-ATP/CoTPP.^[52] The angle between these planes is 118 and 121° for the uncomplexed and fullerene-complexed zinc compounds, which correspond to quadratic-pyramidal and octahedral ligand spheres, respectively. Moreover, the investigated structures show differences with respect to the axial metal–nitrogen bond lengths: the DFT optimization yields for 4-ATP/ZnTPP a distance of 2.26 Å between the zinc atom and the 4-ATP nitrogen atom. The addition of a second axial ligand, that is, the PyC₆₀ linker, leads to a stretching of

Table 1. BP/SV(P) optimized molecular geometrical parameters for 4-ATP/ZnTPP/PyC₆₀.

	4-ATP/ZnTPP	4-ATP/ZnTPP/PyC ₆₀
Zn–N _{ATP} –C _{ATP}	118°	121°
Zn–N _{ATP}	2.26 Å	2.70 Å
Zn–N _{PYR}	–	2.26 Å
Zn–N _{POR}	2.08 Å, 2.10 Å	2.09 Å, 2.10 Å
Zn–C ₆₀	–	15.27 Å
O–C–C–O	–	178°

these bonds to 2.70 Å, as to be expected for such an electron-rich complex. When an empirical dispersion correction^[53] is added, this bond length reduces to 2.5 Å. The interatomic distances between the metal atom and the nitrogen atom located on the pyridinyl ligand is 2.26 Å, whereas the in-plane metal–nitrogen bonds of all compounds are almost equal (with values between 2.08 and 2.10 Å). The linker chain adopts an almost linear configuration with an O–C–O dihedral angle of 178°, and the Zn–C₆₀ distance is 15.27 Å.

2.2.2. Molecular Orbitals

Figure 6 shows the density of states (DOS) and the frontier orbitals of the 4-ATP/ZnTPP (left) and 4-ATP/ZnTPP/PyC₂C₆₀ (right) structures obtained from B3LYP/SV(P) single-point calculations using the BP/SV(P) optimized geometries. Near the peaks in the density of states we also report the subsystem where the state is localized. The DOS was obtained by using a constant Gaussian broadening for each molecular orbital.

For 4-ATP/ZnTPP, the HOMO and LUMO are π orbitals located on the porphyrin ring. The LUMO is (almost) twofold degenerate. Lower-energy states (–5.7 eV) are located on 4-ATP/ZnTPP. The computed Kohn–Sham energy gap is 2.66 eV.

The HOMO of 4-ATP/ZnTPP/PyC₂C₆₀ closely resembles the HOMO of 4-ATP/ZnTPP and is shifted up in energy by 0.13 eV due to the interaction with PyC₂C₆₀. On the other hand, the (almost threefold degenerate) LUMO of 4-ATP/ZnTPP/PyC₂C₆₀ is completely localized on the fullerene moiety. The energy of the LUMO is much lower than that of the LUMO of 4-ATP/ZnTPP, and thus, the Kohn–Sham energy gap is reduced to 1.27 eV. Lower-energy states are localized on 4-ATP (–5 eV) and on the fullerene (–5.9 eV). This last state (not shown) resembles the HOMO of an isolated fullerene. Higher-energy states are localized on the fullerene (–2.5 eV) and on the porphyrin ring (–2.2 eV). The latter state (not shown) resembles the LUMO of the 4-ATP/ZnTPP shown at the left-upper corner of Figure 6. The computed energy gap is in agreement with electrochemical measurements on similar systems.^[18]

3. Discussion

The most significant result of this work is the observation of molecular rectification by 4-ATP/ZnTPP/PyC₂C₆₀ (hereafter denoted for simplicity as ZnTPP/PyC₂C₆₀) compared to symmetric *I/V* curves for 4-ATP/ZnTPP (hereafter denoted for simplicity as ZnTPP). Tunneling is easier for electrons moving from the ac-

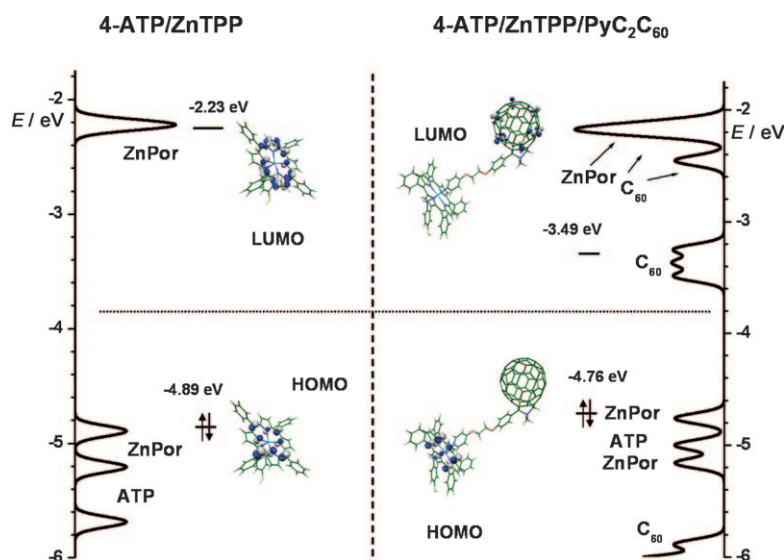


Figure 6. B3LYP density of states (Gaussian broadened), HOMO and LUMO wavefunctions and eigenvalues for 4-ATP/ZnTPP/PyC₂C₆₀ (left) and 4-ATP/ZnTPP/PyC₂C₆₀ (right). Labeling of the states refers to their localization on the porphyrin (ZnPor), aminothiophenol (ATP), and fullerene (C₆₀) subunits. The Fermi level (E_f) is indicated as a dashed–dotted line.

ceptor side of the dyads to the donor side; this is the opposite sense from that reported by Nishino et al. for porphyrins and fullerenes in tunneling contact. On the other hand, our results are consistent with recent investigations of Wang et al.,^[40] who investigated pyridyl azafulleroid oligomers using STS, and Honciuc et al.,^[44] who studied Langmuir–Schaefer monolayers of fullerene bis-malonate. Honciuc et al. found higher current at (small) positive voltage from the donor side.

For quantitative analysis of the *I/V* curves of ZnTPP and ZnTPP/PyC₂C₆₀, we first employ the Landauer formula [in atomic units, Eq. (1)]:

$$I(V) = \frac{1}{\pi} \int [f_s(\varepsilon, \mu_s) - f_t(\varepsilon, \mu_t)] T(\varepsilon, V) d\varepsilon \quad (1)$$

where $\mu_s = E_f + |e|V/2$ and $\mu_t = E_f - |e|V/2$ (E_f is the energy of the Fermi level).

We approximate the transmission coefficient as Equation (2):^[54]

$$T(\varepsilon, V) = \sum_X n_X \frac{\Gamma_{XT} \Gamma_{XS}}{\Gamma_{XT} + \Gamma_{XS}} g(\varepsilon; E_X, \Gamma_{XT} + \Gamma_{XS}) \quad (2)$$

where X runs over the frontier orbitals, that is, HOMO and LUMO of the donor (for ZnTPP) or HOMO and LUMO of the donor and the acceptor (for ZnTPP/PyC₂C₆₀), and n_X is the orbital degeneracy (e.g. three for the LUMO of the fullerene), $g(\varepsilon; \varepsilon_0, \Gamma) = (\Gamma/2\pi)/[(\varepsilon - \varepsilon_0)^2 + (\Gamma/2)^2]$ is the Lorentzian function, and Γ_{XS} and Γ_{XT} represent the coupling between orbital X and the substrate/tip, respectively.

The eigenvalues entering Equation (2) require several considerations. The correct eigenvalues to be used in a molecular transport calculation are the quasiparticle levels, that is, the en-

ergies required to add or remove an electron, which also includes the coupling to the substrate, that is, the image potential.^[30,55,56] These quantities are very difficult to compute even for the smallest systems, so that usually energy levels from DFT in local-density approximation (LDA) are used in molecular transport calculations.^[57] However the LDA energy gap strongly underestimates the quasiparticle energy gap of molecules in the gas phase due to the exchange-correlation discontinuity.^[58] When the molecules are coupled to metal substrates the quasiparticle gap decreases due to the increased environment polarization, but it is still much larger than the LDA.^[55,56] A more accurate energy gap can be obtained in the framework of a hybrid DFT^[66] scheme such as that employed here. We use for E_x the B3LYP eigenvalues for the isolated molecule reported in Figure 6. To quantify the effect of the substrate on the frontier eigenvalues (i.e. orbital shifts due to chemical interactions and image-potential effects), the computation of the molecule on a large gold cluster or using periodic boundary conditions (e.g. see refs. [31,38]) is required. Due to the size of our system, such simulations are computationally too expensive; moreover, coupling to the substrate is expected to be very similar in ZnTPP and ZnTPP/PyC₂C₆₀. Thus, this should only cause a rigid shift of the eigenvalues of the molecular orbitals without modifying the main differences between the two systems. We thus neglect this shift of eigenvalues towards the metal Fermi level, and in the following we use the Fermi level of the molecule instead.

Molecular orbital eigenvalues are also expected to be dependent on the applied voltage. In the case of donor–acceptor systems with large spatial separation of the corresponding subunits, such as the system investigated in this work, the Datta model^[59] which assumes the same voltage dependence for all orbitals, cannot be used. Herein, we model the voltage dependence of the orbital energies as Equation (3):

$$E_x = E_x(V) = E_{x0} - |e| \left(\frac{V}{2} - \frac{z_x}{z_T} V \right) \quad (3)$$

where E_{x0} is the eigenvalue at equilibrium computed from DFT (see Figure 6), z_x the distance of the center of mass of molecular orbital x from the substrate, and z_T is the resulting tip–substrate distance. Equation (3) assumes that the molecular orbital x feels the electrostatic potential at its center of mass z_x . In this way the HOMO and the LUMO orbitals will have a different voltage dependence due to different localization in space. The Datta model is recovered in Equation (3) if all molecular orbitals are located at $z_x = \eta z_T$. For $\eta = 0.5$ the eigenvalues do not depend on the voltage and the I/V curves are always symmetric.^[59]

For ZnTPP, we assume a distance of 15 Å between the tip and the center of the porphyrin: the resulting tip–substrate distance is thus $z_T = 23$ Å. For ZnTPP/PyC₂C₆₀, the tip distance is only 5 Å larger, as obtained from STM measurements (see Figure 3). The increased tip distance is much smaller than the real height of PyC₂C₆₀ due to the smaller conductivity of ZnTPP/PyC₂C₆₀ with respect to ZnTPP.

To verify the accuracy of Equation (3) in describing the real potential drop in the STM junction, we performed DFT calculations under an external uniform electric field. Results are shown in Figure 7, which shows the HOMO and LUMO eigen-

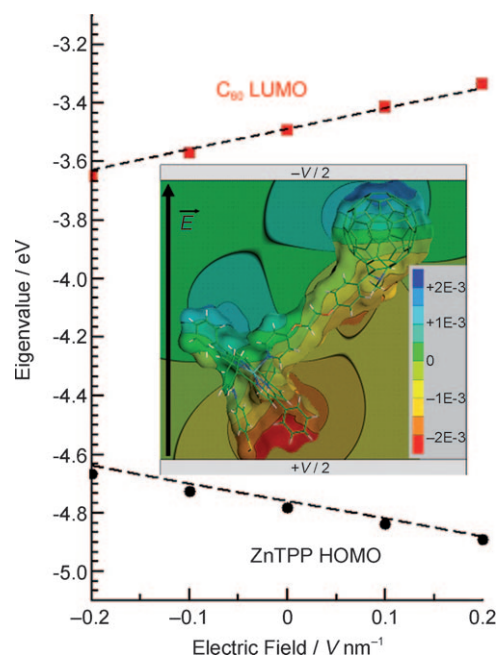


Figure 7. Computed HOMO (black circles) and LUMO (red squares) eigenvalues as a function of the applied external electric field. Dashed lines (---): eigenvalues computed from Equation (3). Inset: electric-field-induced molecular electrostatic potential (see text).

values (black circles and red squares, respectively) as a function of the applied external field, as well as the eigenvalues computed from Equation (3) (dashed lines). The excellent agreement confirms the validity of Equation (3) in describing the electric field effect for this donor–acceptor system. Figure 7 also shows that the energy gap decreases for negative substrate bias (see also below). The inset of Figure 7 shows the electric field induced molecular electrostatic potential (i.e. obtained from Mulliken atomic charge differences with and without the external applied field). Despite the complexity of this system, a linear drop can be seen in the fullerene and in the porphyrin subsystem.

Figure 8a shows the results for ZnTPP using the above Landauer model. We use $z_{D,HOMO} = z_{D,LUMO} = 8$ Å (see Figure 5), that is, the HOMO and the LUMO of ZnTPP are localized in the same region of space. The I/V curve with a Fermi level located in the center of the HOMO–LUMO gap (i.e. -3.6 eV) is fully symmetric and in better agreement with the experiment (the energy gap in experiments is a bit smaller, probably due to overestimation of the computed energy gap). Note that we do not shift the absolute value of the Fermi level of the molecule to match the Fermi level of the gold electrode. If the Fermi level is shifted down towards the HOMO, the I/V curves become more asymmetric with larger current at negative volt-

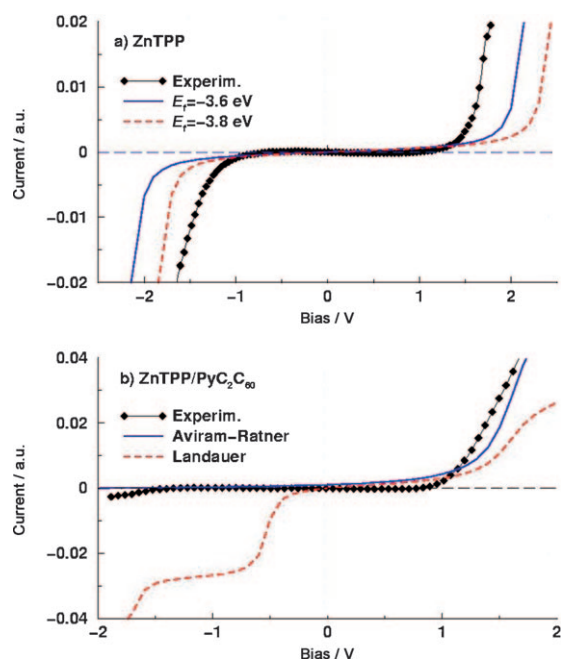


Figure 8. *I/V* curves for a) ZnTPP and b) ZnTPP/PyC₆₀ from different models: a) Landauer model with $E_f = -3.8$ eV (red dashed line) and $E_f = -3.6$ eV (blue solid line). b) Landauer model with $E_f = -3.8$ eV (red dashed line) and Aviram–Ratner model with $E_f = -3.8$ eV (blue solid line). Coupling parameters: $\Gamma_{DS} = \Gamma_{AT} = 0.1$, $\Gamma_{DT} = \Gamma_{AT} = 0.001$.

age. We can thus conclude that the Fermi level of ZnTPP is located very close to the middle of the energy gap.

The computed *I/V* curve for ZnTPP/PyC₆₀ (see Figure 8b, red dashed line) is asymmetric with larger current at negative voltage. The curve in Figure 8b was obtained with $E_f = -3.8$ eV (see below), but the *I/V* curve remains asymmetric even with the Fermi level located in the middle of the HOMO–LUMO gap. This asymmetry is related to the spatial separation of HOMO and LUMO. In fact the LUMO of the acceptor is at $z_{A,LUMO} = 21$ Å (see Figure 5), that is, very close to the STM tip, while the HOMO of the donor is again at $z_{D,HOMO} = 8$ Å. Thus, at negative substrate voltage the energy of the LUMO decreases while the energy of the HOMO increases: this results in a reduced energy gap and thus in a higher current at negative substrate bias.^[29,32] Thus, larger currents are obtained at negative bias, whichever is the Fermi level (see Figure S2 of the Supporting Information). This situation is similar to that reported by Nishino et al.,^[26] in which the fullerene is connected to the STM tip and thus the eigenvalue of the LUMO shifts with the applied bias.

Our experimental results, like those of Wang et al.^[40] and Honciuc et al.,^[44] cannot be explained by an elastic resonant tunneling process as described by the Landauer formula [Eq. (1)]. As an alternative we consider the Aviram–Ratner model, in which acceptor and donor molecules are linked by a bridge consisting of π bonds, and the LUMO and HOMO are well separated. When the Fermi level E_f is in close proximity to the LUMO, a relatively small negative bias applied to the acceptor-side electrode (i.e. a positive substrate bias) brings the LUMO into resonance. Krzeminski et al.^[30] showed that different

behaviors result for acceptor and donor moieties linked by a π bond if the HOMO and LUMO are delocalized. In that case initial lineup with the Fermi level close to the LUMO leads to rectification in the opposite sense of the Aviram–Ratner model, that is, negative sample bias corresponds to easy current flow. Our calculations, presented in Figure 6, show that the LUMO and the HOMO of the dyads are localized on the fullerene and porphyrin moieties, respectively. From such a picture, we expect these molecular orbitals to be involved in the rectification process in the manner suggested by Aviram and Ratner: in the STM junction, under positive sample bias, the LUMO of the fullerene (A) will come into resonance with the Fermi level of the tip, thus allowing an electron to flow into the LUMO. Using the same principle, an electron will resonantly tunnel from the HOMO of the porphyrin (D) to the Fermi level of the substrate. According to the Aviram–Ratner model for rectification processes, this will create D^+/A^- species. Finally, an electron transfer from the reduced acceptor A^- to the oxidized donor D^+ will occur, thus allowing an intramolecular charge transfer reaction $D^+/A^- \rightarrow D/A$. Under negative sample bias, the LUMO of A and the HOMO of D are too far from the Fermi level of the tip and the substrate for resonant tunneling to be energetically allowed, thus resulting in a negligible current (as illustrated in Figure 9).

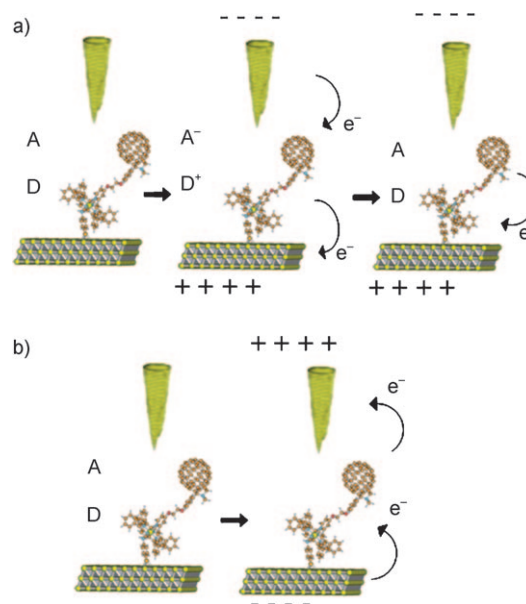


Figure 9. Schematic picture of the Aviram–Ratner electron-transfer mechanism involving ZnTPP/PyC₆₀ dyads on Au(111) and the STM tip: a) forward- and b) reverse-bias process.

The above Aviram–Ratner description requires a Fermi level close to the LUMO. First-principles calculations of the Fermi level, which requires inclusion of the molecule linked to the metal substrate, are out of reach for large systems like our ZnTPP/PyC₆₀ complex. However the following discussion sheds some light on the position of the Fermi level.

Considering that each molecular orbital is broadened due to coupling to the metal substrate, the Fermi level E_f^D of the

donor (ZnTPP) system can be computed^[56] from Equation (4):

$$N_D = \int_{-\infty}^{E_f^D} \sum_{i \in D} 2g(\varepsilon; \varepsilon_i^D, \Gamma_i^D) d\varepsilon = \sum_{i \in D} 1 + \frac{2}{\pi} \tan^{-1} \left(\frac{\varepsilon_i^D - E_f^D}{\Gamma_i^D/2} \right) \quad (4)$$

where $g(\varepsilon; \varepsilon_0, \Gamma) = (\Gamma/2\pi)/[(\varepsilon - \varepsilon_0)^2 + (\Gamma/2)^2]$ is the Lorentzian function, Γ_i^D the broadening of the energy level located at ε_i^D , and N_D the number of electrons in the molecules. If all Γ_i vanish, then the Fermi level is located in the middle of the energy gap.

In the same way, the Fermi level of a weakly interacting donor–acceptor system $E_f^{A/D}$ can be determined from Equation (5):

$$N_A + N_D = \sum_{i \in D} 1 + \frac{2}{\pi} \tan^{-1} \left(\frac{\varepsilon_i^D - E_f^{A/D}}{\Gamma_i^D} \right) + \sum_{i \in A} 1 + \frac{2}{\pi} \tan^{-1} \left(\frac{\varepsilon_i^A - E_f^{A/D}}{\Gamma_i^A} \right) \quad (5)$$

In our STM configuration (see Figure 5), we have $\Gamma_i^A \ll \Gamma_i^D$ due to the larger distance between the fullerene and the substrate. As a first approximation, we set $\Gamma_i^A \approx 0$ and obtain Equation (6):

$$N_A + N_D \approx \sum_{i \in D} 1 + \frac{2}{\pi} \tan^{-1} \left(\frac{\varepsilon_i^D - E_f^{A/D}}{\Gamma_i^D} \right) + \sum_{i \in A} \theta(\varepsilon_i^A - E_f^{A/D}) \quad (6)$$

where θ is the unitary step function. The second term on the right-hand side is equal to N_D : we thus obtain from Equation (1) that $E_f^{A/D} \approx E_f^D$. This means that to a first approximation, the Fermi levels for the ZnTPP and ZnTPP/PyC₂C₆₀ systems are the same due to negligible coupling of the fullerene with the substrate. In Figure 6, we draw the Fermi level at -3.8 eV; this corresponds to a position nearly in the middle of the energy gap for ZnTPP (see discussion above) and very close to the LUMO for the ZnTPP/PyC₂C₆₀.

The Aviram–Ratner conduction mechanism can be quantitatively described by Equation (7).^[60]

$$I = I_0 \int \zeta_{AT}(\varepsilon) f_T(\varepsilon, \mu_T) d\varepsilon \int \zeta_{DS}(\varepsilon) [1 - f_S(\varepsilon, \mu_S)] d\varepsilon - I_0 \int \zeta_{DS}(\varepsilon) f_S(\varepsilon, \mu_S) d\varepsilon \int \zeta_{AT}(\varepsilon) [1 - f_T(\varepsilon, \mu_T)] d\varepsilon \quad (7)$$

where $\zeta_{AT}(\varepsilon) = g(\varepsilon; E_A(V); \Gamma_{AT})$, $\zeta_{DS}(\varepsilon) = g(\varepsilon; E_D(V); \Gamma_{DS})$, and I_0 takes into account the donor–acceptor transfer rate. We assume a linear voltage drop across the junction [see Eq. (3)]. The computed I/V curve for ZnTPP/PyC₂C₆₀ is shown as a blue solid line in Figure 8b. It shows a large current at positive substrate voltage and is in close agreement with the experimental results. On increasing the tip–molecule distance only the current onset changes, and thus this parameter does not affect the rectification direction (see Figure S3 of the Supporting Information).

Finally, we note that at large negative substrate bias (-1.5 eV) the experimental current starts to deviate from zero. This current cannot be related to the inverse Aviram–Ratner process, which is expected to occur only above 6 eV. Instead, we assign this current to resonant tunneling (Landauer), which is enhanced at negative bias, as described above. Thus, both Landauer and Aviram–Ratner processes can be present in a donor–acceptor system. The predominance of the former or the latter depends on the molecular structure and/or the Fermi level and/or the tip–molecule distance.^[26,40,44]

Conclusions

Supramolecular axially ligated ZnTPP/PyC₂C₆₀ dyads, prepared ex situ on a gold(111) surface through simple and inexpensive wet processing techniques, show molecular rectification with high tunneling currents at positive substrate voltage, with electron tunneling from the acceptor to the donor moieties of the dyads. Ultrahigh-vacuum scanning tunneling microscopy and spectroscopy measurements show bias-dependent apparent heights of the dyads and asymmetric I/V curves. Density functional calculations confirm almost complete localization of HOMO and LUMO levels on donor and acceptor moieties, and suggest that the Fermi level is very close to the LUMO level of ZnTPP/PyC₂C₆₀. This alignment is consistent with the observed inverse sense of rectification within the Aviram–Ratner mechanism.

Experimental Section

We synthesized zinc(II) 10,15,20-tetraphenyl-21*H*,23*H*-porphine (ZnTPP) and *N*-methyl-3,4-fulleropyrrolidine bearing a *p*-diethoxy-pyridyl group (PyC₂C₆₀) by following standard procedures.^[46,61] 4-Aminothiophenol (4-ATP, 90%, Aldrich) was used as received. The molecular structures of 4-ATP, ZnTPP, and PyC₂C₆₀ are reported in Figure 1. We used as substrates atomically flat Au(111) on mica, acquired from Molecular Imaging. All solvents used were of analytical grade. We prepared metal porphyrin/fulleropyrrolidine (ZnTPP/PyC₂C₆₀) dyads by anchoring PyC₂C₆₀ to a self-assembled monolayer of ZnTPPs via axial ligation. The 4-ATP/ZnTPP self-assembled monolayer (ZnTPP SAM) was produced by incubating bare Au(111) in a solution of 4-ATP in ethanol followed by a solution of ZnTPP in chloroform.^[52,62] Subsequently, the PyC₂C₆₀ molecules were anchored to form dyads by dipping the ZnTPP SAM into a 10^{-7} M solution of PyC₂C₆₀ in toluene for approximately 20 s. Then, the sample was rinsed in warm toluene to remove excess PyC₂C₆₀. During this process, the MTPP ring is assumed to weaken the interaction with the 4-ATP amino group and create a stable axial link with the pyridyl moiety of PyC₂C₆₀. In addition, since no detachment of the dyad from the substrate is observed after washing and no ligand field stabilization effect in Zn²⁺ ions (due to their completed *d* shell) fixes precisely the stereochemistry of these compounds,^[63] a weakly six coordinate Zn²⁺ assembly could be hypothesized. Shortly after preparation, the sample was inserted into the UHV system and then annealed to break up any fullerene aggregates. The STM and STS measurements were carried out in an Omicron VT-STM in UHV (10^{-10} mbar) at room temperature with both W and Pt/Ir tips. We acquired STS curves in a closely spaced grid including topographic features which we identify as dyads and uncomplexed

ZnTPP. A large number of spectra were acquired from multiple positions on different samples to check for their reproducibility.

The geometries of 4-ATP/ZnTPP and 4-ATP/ZnTPP/PyC₂C₆₀ were fully optimized without any symmetry restrictions at the DFT level with the Becke–Perdew (BP)^[64,65] exchange–correlation functional. Single-point calculations for 4-ATP/ZnTPP and 4-ATP/ZnTPP/PyC₂C₆₀ were performed with the B3LYP^[66,67] functional. All calculations were carried out with the TURBOMOLE 5.7^[68] program package, the standard SV(P)^[69] basis set, and the default m3 numerical quadrature grid.

Acknowledgements

This work was supported by CNR-INFM, by an NSF US–Italy Cooperative Research Program No. OISE-0242579, by the SpiDME European project, by the ERC-Starting Grant FP7-Project “DEDOM”, Grant agreement No. 207441, and by MIUR FIRB 2003 “SYNERGY” grant. We thank E. Fabiano for discussions, R. Ahlrichs for providing us with the TURBOMOLE program package, and the SPACI consortium for the computational infrastructure support. R. J. Phaneuf acknowledges support from a National Science Foundation (NSF) international grant (No. OISE0242579) and from NSF-MRSEC (DMR-0080008).

Keywords: donor–acceptor systems • fullerenes • molecular electronics • porphyrinoids • scanning probe microscopy

- [1] A. H. Flood, J. F. Stoddart, D. W. Steuerman, J. R. Heath, *Science* **2004**, 306, 2055.
- [2] C. Joachim, J. K. Gimzewski, A. Aviram, *Nature* **2000**, 408, 541.
- [3] G. Maruccio, R. Cingolani, R. Rinaldi, *J. Mater. Chem.* **2004**, 14, 542.
- [4] A. Nitzan, M. A. Ratner, *Science* **2003**, 300, 1384.
- [5] H. Imahori, *Org. Biomol. Chem.* **2004**, 2, 1425.
- [6] F. D'Souza, G. R. Deviprasad, M. S. Rahman, J. P. Choi, *Inorg. Chem.* **1999**, 38, 2157.
- [7] H. Ajie, M. M. Alvarez, S. J. Anz, R. D. Beck, F. Diederich, K. Fostiropoulos, D. R. Huffman, W. Kratschmer, Y. Rubin, K. E. Schriver, D. Sensharma, R. L. Whetten, *J. Phys. Chem.* **1990**, 94, 8630.
- [8] W. Kratschmer, K. Fostiropoulos, D. R. Huffman, *Chem. Phys. Lett.* **1990**, 170, 167.
- [9] W. Kratschmer, L. D. Lamb, K. Fostiropoulos, D. R. Huffman, *Nature* **1990**, 347, 354.
- [10] Q. S. Xie, E. Perezcordero, L. Echegoyen, *J. Am. Chem. Soc.* **1992**, 114, 3978.
- [11] R. Marczak, V. Sgobba, W. Kutner, S. Gadde, F. D'Souza, D. M. Guldi, *Langmuir* **2007**, 23, 1917.
- [12] T. Hasobe, H. Imahori, P. V. Kamat, T. K. Ahn, S. K. Kim, D. Kim, A. Fujimoto, T. Hirakawa, S. Fukuzumi, *J. Am. Chem. Soc.* **2005**, 127, 1216.
- [13] M. E. El-Khouly, L. M. Rogers, M. E. Zandler, G. Suresh, M. Fujitsuka, O. Ito, F. D'Souza, *ChemPhysChem* **2003**, 4, 474.
- [14] F. D'Souza, G. R. Deviprasad, M. E. El-Khouly, M. Fujitsuka, O. Ito, *J. Am. Chem. Soc.* **2001**, 123, 5277.
- [15] F. D'Souza, G. R. Deviprasad, M. E. Zandler, M. E. El-Khouly, M. Fujitsuka, O. Ito, *J. Phys. Chem. A* **2003**, 107, 4801.
- [16] F. D'Souza, P. M. Smith, M. E. Zandler, A. L. McCarty, M. Itou, Y. Araki, O. Ito, *J. Am. Chem. Soc.* **2004**, 126, 7898.
- [17] F. D'Souza, R. Chitta, S. Gadde, M. E. Zandler, A. S. D. Sandanayaka, Y. Araki, O. Ito, *Chem. Commun.* **2005**, 1279.
- [18] F. D'Souza, G. R. Deviprasad, M. E. Zandler, V. T. Hoang, A. Klykov, M. VanStipdonk, A. Perera, M. E. El-Khouly, M. Fujitsuka, O. Ito, *J. Phys. Chem. A* **2002**, 106, 3243.
- [19] D. I. Schuster, P. Cheng, P. D. Jarowski, D. M. Guldi, C. P. Luo, L. Echegoyen, S. Pyo, A. R. Holzwarth, S. E. Braslavsky, R. M. Williams, G. Klihm, *J. Am. Chem. Soc.* **2004**, 126, 7257.
- [20] N. V. Tkachenko, H. Lemmetyinen, J. Sonoda, K. Ohkubo, T. Sato, H. Imahori, S. Fukuzumi, *J. Phys. Chem. A* **2003**, 107, 8834.
- [21] H. Imahori, N. V. Tkachenko, V. Vehmanen, K. Tamaki, H. Lemmetyinen, Y. Sakata, S. Fukuzumi, *J. Phys. Chem. A* **2001**, 105, 1750.
- [22] S. Fukuzumi, H. Imahori, H. Yamada, M. E. El-Khouly, M. Fujitsuka, O. Ito, D. M. Guldi, *J. Am. Chem. Soc.* **2001**, 123, 2571.
- [23] V. Chukharev, N. V. Tkachenko, A. Efimov, D. M. Guldi, A. Hirsch, M. L. Scheloske, H. Lemmetyinen, *J. Phys. Chem. B* **2004**, 108, 16377.
- [24] H. Yamada, H. Imahori, S. Fukuzumi, *J. Mater. Chem.* **2002**, 12, 2034.
- [25] V. Chukharev, T. Vuorinen, A. Efimov, N. V. Tkachenko, M. Kimura, S. Fukuzumi, H. Imahori, H. Lemmetyinen, *Langmuir* **2005**, 21, 6385.
- [26] T. Nishino, T. Ito, Y. Umezawa, *Proc. Natl. Acad. Sci. USA* **2005**, 102, 5659.
- [27] R. M. Metzger, B. Chen, U. Hopfner, M. V. Lakshmikantham, D. Vuillaume, T. Kawai, X. L. Wu, H. Tachibana, T. V. Hughes, H. Sakurai, J. W. Baldwin, C. Hosch, M. P. Cava, L. Brehmer, G. J. Ashwell, *J. Am. Chem. Soc.* **1997**, 119, 10455.
- [28] A. C. Brady, B. Hodder, A. S. Martin, J. R. Sambles, C. P. Ewels, R. Jones, P. R. Briddon, A. M. Musa, C. A. F. Panetta, D. L. Mattern, *J. Mater. Chem.* **1999**, 9, 2271.
- [29] J. C. Ellenbogen, J. C. Love, *Proc. IEEE* **2000**, 88, 386.
- [30] C. Krzeminski, C. Delerue, G. Allan, D. Vuillaume, R. M. Metzger, *Phys. Rev. B* **2001**, 64, 085405.
- [31] S. Q. Zhou, Y. Q. Liu, W. F. Qiu, Y. Xu, X. B. Huang, Y. S. Li, L. Jiang, D. B. Zhu, *Adv. Funct. Mater.* **2002**, 12, 65.
- [32] K. Stokbro, J. Taylor, M. Brandbyge, *J. Am. Chem. Soc.* **2003**, 125, 3674.
- [33] R. M. Metzger, J. W. Baldwin, W. J. Shumate, I. R. Peterson, P. Mani, G. J. Mankey, T. Morris, G. Szulcowski, S. Bosi, M. Prato, A. Comito, Y. Rubin, *J. Phys. Chem. B* **2003**, 107, 1021.
- [34] F. Jackel, Z. Wang, M. D. Watson, K. Mullen, J. P. Rabe, *Chem. Phys. Lett.* **2004**, 387, 372.
- [35] G. J. Ashwell, A. Chwialkowska, L. R. H. High, *J. Mater. Chem.* **2004**, 14, 2389.
- [36] G. J. Ashwell, A. Chwialkowska, L. R. H. High, *J. Mater. Chem.* **2004**, 14, 2848.
- [37] G. J. Ashwell, W. D. Tyrrell, A. J. Whittam, *J. Am. Chem. Soc.* **2004**, 126, 7102.
- [38] A. Honciuc, A. Jaiswal, A. Gong, H. Ashworth, C. W. Spangler, I. R. Peterson, L. R. Dalton, R. M. Metzger, *J. Phys. Chem. B* **2005**, 109, 857.
- [39] M. Elbing, R. Ochs, M. Koentopp, M. Fischer, C. von Hanisch, F. Weigend, F. Evers, H. B. Weber, M. Mayor, *Proc. Natl. Acad. Sci. USA* **2005**, 102, 8815.
- [40] B. Wang, Y. S. Zhou, X. L. Ding, K. D. Wang, X. P. Wang, J. L. Yang, J. G. Hou, *J. Phys. Chem. B* **2006**, 110, 24505.
- [41] B. Mukherjee, K. Mohanta, A. J. Pal, *Chem. Mater.* **2006**, 18, 3302.
- [42] G. J. Ashwell, W. D. Tyrrell, B. Urasinska, C. S. Wang, M. R. Bryce, *Chem. Commun.* **2006**, 1640.
- [43] X. Yin, H. M. Liu, J. Zhao, *J. Chem. Phys.* **2006**, 125, 094711.
- [44] A. Honciuc, R. M. Metzger, A. J. Gong, C. W. Spangler, *J. Am. Chem. Soc.* **2007**, 129, 8310.
- [45] A. Aviram, M. A. Ratner, *Chem. Phys. Lett.* **1974**, 29, 277.
- [46] P. Rothmund, *J. Am. Chem. Soc.* **1936**, 58, 625.
- [47] X. H. Lu, M. Grobis, K. H. Khoo, S. G. Louie, M. F. Crommie, *Phys. Rev. Lett.* **2003**, 90, 096802.
- [48] J. I. Pascual, J. Gomez-Herrero, C. Rogero, A. M. Baro, D. Sanchez-Portal, E. Artacho, P. Ordejon, J. M. Soler, *Chem. Phys. Lett.* **2000**, 321, 78.
- [49] T. A. Jung, R. R. Schlittler, J. K. Gimzewski, H. Tang, C. Joachim, *Science* **1996**, 271, 181.
- [50] N. D. Lang, *Phys. Rev. B* **1987**, 36, 8173.
- [51] X. H. Lu, M. Grobis, K. H. Khoo, S. G. Louie, M. F. Crommie, *Phys. Rev. Lett.* **2003**, 90, 096802.
- [52] V. Arima, E. Fabiano, R. I. R. Blyth, F. Delia Sala, F. Martino, J. Thompson, R. Cingolani, R. Rinaldi, *J. Am. Chem. Soc.* **2004**, 126, 16951.
- [53] S. Grimme, *J. Comput. Chem.* **2004**, 25, 1463.
- [54] B. Larade, A. M. Bratkovsky, *Phys. Rev. B* **2003**, 68, 235305.
- [55] J. B. Neaton, M. S. Hybertsen, S. G. Louie, *Phys. Rev. Lett.* **2006**, 97, 216405.
- [56] J. D. Sau, J. B. Neaton, H. J. Choi, S. G. Louie, M. L. Cohen, *Phys. Rev. Lett.* **2008**, 101, 026804.
- [57] J. Taylor, M. Brandbyge, K. Stokbro, *Phys. Rev. Lett.* **2002**, 89, 138301.
- [58] M. L. J. P. Perdew, *Phys. Rev. Lett.* **1983**, 51, 1884.

- [59] S. Datta, W. D. Tian, S. H. Hong, R. Reifenger, J. I. Henderson, C. P. Kubiak, *Phys. Rev. Lett.* **1997**, 79, 2530.
- [60] K. Walczak, Arxiv preprint **2003**, cond-mat/0305493.
- [61] G. Vasapollo, G. Mele, L. Longo, R. Ianne, B. G. Gowenlock, K. G. Orrell, *Tetrahedron Lett.* **2002**, 43, 4969.
- [62] V. Arima, F. Matino, J. Thompson, R. Del Sole, G. Mele, G. Vasapollo, R. Cingolani, R. Rinaldi, R. I. R. Blyth, *Appl. Surf. Sci.* **2005**, 248, 40.
- [63] F. A. Cotton, G. Wilkinson, *Advanced Inorganic Chemistry*, 5th ed., Wiley, New York, **1988**, p. 598.
- [64] A. D. Becke, *Phys. Rev. A* **1988**, 38, 3098.
- [65] J. P. Perdew, *Phys. Rev. B* **1986**, 33, 8822.
- [66] A. D. Becke, *J. Chem. Phys.* **1993**, 98, 5648.
- [67] C. Lee, W. Yang, R. G. Parr, *Phys. Rev. B* **1988**, 37, 785.
- [68] R. Ahlrichs, TURBOMOLE, Version 5.8, Karlsruhe, **2005**.
- [69] A. Schäfer, H. Horn, R. Ahlrichs, *J. Chem. Phys.* **1992**, 97, 2571.

Received: May 13, 2009

Published online on September 23, 2009